Interfacial reaction in the growth of epitaxial Sr Ti O 3 thin films on (001) Si substrates

J. Q. He, C. L. Jia, V. Vaithyanathan, D. G. Schlom, J. Schubert, A. Gerber, H. H. Kohlstedt, and R. H. Wang

---

Articles you may be interested in

Studies of the interfacial structure of La Al O 3 thin films on silicon by x-ray reflectivity and angle-resolved x-ray photoelectron spectroscopy
J. Appl. Phys. **97**, 124104 (2005); 10.1063/1.1941470

Extended defects in epitaxial Sc 2 O 3 films grown on (111) Si
Appl. Phys. Lett. **86**, 051901 (2005); 10.1063/1.1857068

Growth and physical properties of Ga 2 O 3 thin films on GaAs(001) substrate by molecular-beam epitaxy
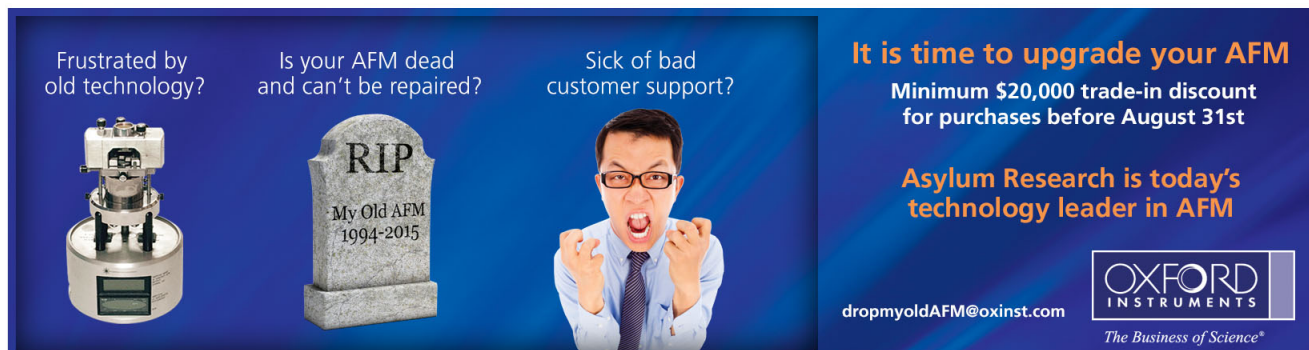Appl. Phys. Lett. **82**, 2978 (2003); 10.1063/1.1572478

Two-dimensional growth of high-quality strontium titanate thin films on Si
J. Appl. Phys. **93**, 4521 (2003); 10.1063/1.1562001

Epitaxial oxide thin films on Si(001)
J. Vac. Sci. Technol. B **18**, 2139 (2000); 10.1116/1.1303737

Interfacial reaction in the growth of epitaxial SrTiO₃ thin films on (001) Si substrates

J. Q. He[a)] and C. L. Jia
Institut für Festkörperforschung, Forschungszentrum Jülich Gesellschaft mit Beschränkter Haftung (GmbH), D-52425 Jülich, Germany

V. Vaithyanathan and D. G. Schlom
Department of Materials Science and Engineering, The Pennsylvania State University, University Park, Pennsylvania 16802-5005

J. Schubert
Institut für Schichten und Grenzflächen, Forschungszentrum Jülich Gesellschaft mit Beschränkter Haftung (GmbH), D-52425 Jülich, Germany

A. Gerber and H. H. Kohlstedt
Institut für Festkörperforschung, Forschungszentrum Jülich Gesellschaft mit Beschränkter Haftung (GmbH), D-52425 Jülich, Germany

R. H. Wang
Department of Physics and Center for Electron Microscopy, Wuhan University, Wuhan 430072, People's Republic of China

The $SrTiO_3/Si$ interface was investigated by transmission electron microscopy for $SrTiO_3$ films grown on (001) Si by molecular-beam epitaxy with different native oxide (SiO_2) removal treatments, and Sr/Ti flux ratios. The interface and film microstructure were independent of the process used to remove the native oxide, but the interface reactivity was dependent on the Sr/Ti flux ratio. A low Sr/Ti flux ratio (~0.8) resulted not only in a layer of amorphous material at the film/substrate interface but also in the formation of crystalline $C49$ $TiSi_2$ precipitates at that interface. These results are consistent with thermodynamic expectations in which it is paramount to maintain separation between TiO_2 and the underlying silicon. © *2005 American Institute of Physics*. [DOI: 10.1063/1.1915519]

I. INTRODUCTION

Crystalline $SrTiO_3$ has been touted as one of the most promising candidates for the replacement of amorphous SiO_2 gate dielectrics in silicon-based metal-oxide-semiconductor field-effect transistors (MOSFETs) due to its high dielectric constant and electronic properties.[1–7] In practice, however, it remains a huge challenge to achieve the required electronic properties to make $SrTiO_3$ a viable gate dielectric for silicon-based MOSFETs.[8–12] The stability, bonding, and microstructure of the interface between the oxide film and the substrate are determined by thermodynamic and kinetic effects. All of these factors influence the electronic properties of the metal-oxide/silicon interface, and thus determine the functionality of electronic oxide device structures on silicon platforms.

$SrTiO_3$ is thermodynamically *unstable* in contact with silicon owing to its strong chemical reactivity with silicon.[13–15] Thermodynamic issues are of greater importance in oxide/silicon systems than in other heteroepitaxial systems, particularly in cases where a high-temperature treatment (~900 °C or higher) is traditionally used to fully activate the implanted dopant species in a self-aligned process.[16,17] Even if this high-temperature step is circum-

vented by avoiding a self-aligned process or employing a gate-last process, the processing temperatures encountered in deposition or postdeposition processing (to achieve the desired electronic performance) can also be high. In the specific case of $SrTiO_3$, processing temperatures of ~600 °C are used to achieve epitaxial $SrTiO_3$ films on (001) Si.[3,4,6,7,18,19]

As interfacial reactions can lead to unwanted interfacial reaction layers with low permittivity that would degrade the device performance, the growth of films must be achieved through special reaction paths which can be provided by molecular-beam epitaxy (MBE). Initially, $SrTiO_3$ thin films were grown on (001) Si using a thick SrO buffer layer typically 10 nm in thickness.[20–23] In the work of McKee and co-workers,[2,5–7] direct deposition of oxide films was achieved by incorporating an interfacial strontium silicide layer, which prevents oxidation of the interface[24] and hence, promotes epitaxy. Since then, many groups have achieved epitaxial growth of $SrTiO_3$ on silicon using very different growth strategies.[3,4,18,19,25–27] Even when epitaxial overgrowth of $SrTiO_3$ on silicon is achieved, however, a reaction might occur below the growing surface at the $SrTiO_3/Si$ interface, as is well known to occur in other epitaxial systems with unstable interfaces.[28–32]

In the present work, we investigate the dependence of the $SrTiO_3/Si$ interface reaction on the flux ratio of Sr/Ti and on the pretreatment of the silicon substrate surface. Two

---

[a)]Author to whom correspondence should be addressed; present address: Biology Department, Brookhaven National Laboratory, 50 Bell Ave, Upton, NY 11973; electronic mail: jhe@bnl.gov

methods were used for the removal of the native oxide from the silicon substrates. The microstructures of these films and the film/substrate interfaces were investigated by means of conventional transmission electron microscopy (TEM) and high-resolution transmission electron microscopy (HRTEM). Our studies are focused on the changes in the film microstructure and film/substrate interface as a function of the two parameters of interest: the native oxide removal process and the Sr/Ti flux ratio.

II. EXPERIMENTAL PROCEDURES

SrTiO$_3$ films were grown using an MBE (EPI 930) system, which was modified for the growth of oxides on silicon.[33] A quartz-crystal microbalance was used to measure the fluxes of the elemental species to be deposited and *in situ* reflection high-energy electron diffraction (RHEED) was used to monitor the growth of the oxide film. A molecular beam of strontium from a conventional effusion cell, a stable titanium flux supplied by a titanium sublimation pump (Ti-Ball),[34] and molecular oxygen were used as the elemental sources for SrTiO$_3$ deposition. The base pressure in the growth chamber was $\sim 2 \times 10^{-9}$ Torr. The substrates were (001) B-doped (*p*-type) silicon wafers cut with an accuracy of $\pm 0.1°$ and 50 or 75 mm in diameter. Prior to loading the silicon substrates into the MBE system, the surface organics were removed by ozone cleaning. The microstructure of three samples, A, B, and C, were investigated. In sample A, the native SiO$_2$ on the silicon surface was removed by a strontium "deoxidation" process, which is explained in Ref. 35. In samples B and C, the native oxide was removed by heating to $\sim 900 °C$ in vacuum. For samples A and B, SrTiO$_3$ films were deposited with a Sr/Ti flux ratio of ~ 1, while for sample C a Sr/Ti flux ratio of ~ 0.8 was used.

The growth process is described in detail elsewhere,[18,27] but in brief it consisted of the following steps. A SiO$_2$-free silicon surface, identified by a sharp double-domain 2×1 Si(001) RHEED pattern, was obtained either through a strontium deoxidation process[35] or heating in ultrahigh vacuum (UHV) to $\sim 900 °C$. Upon the clean (001) Si surface at a substrate temperature of 700 °C (measured by an optical pyrometer), a strontium dose of 3.4×10^{14} at./cm^2 [one-half a monolayer[36] (ML) of strontium] was deposited from a strontium MBE source at a flux of $(3-4) \times 10^{13}$ at./cm^2/s. This formed an interfacial strontium silicide layer[2,5,6] that functions to protect the underlying silicon from oxidation and thus preserve an epitaxial template for epitaxial-oxide overgrowth.[24] The wafer was then cooled to near room temperature (under 200 °C), where in UHV an additional $\frac{1}{2}$ ML $(3.4 \times 10^{14}$ at./cm$^2)$ of strontium was deposited. Unlike the strontium deposited at high temperature, which forms strontium silicide,[2,5,6] this room-temperature-deposited strontium layer remains metallic and enables moving a little farther away from the interface before exposing the wafer to oxygen. This helps to avoid oxidizing the underlying silicon. With the substrate still at approximately room temperature (under 200 °C), oxygen was then introduced to a background pressure of $(4-5) \times 10^{-8}$ Torr and additional strontium was deposited in the presence of the oxygen to form

2–3 MLs of SrO. The $\frac{1}{2}$ ML of metallic strontium deposited prior to the oxygen exposure also gets oxidized during this process and becomes an integral part of the epitaxial SrO on silicon. The thickness of the epitaxial SrO layer on silicon is limited to its critical thickness value of ~ 3 MLs (based on the observations of the RHEED patterns), due to the 5% lattice mismatch between SrO and silicon. On top of the crystalline SrO layers, 1–2 MLs of amorphous TiO$_2$ were deposited in an oxygen background pressure of $(1-2) \times 10^{-7}$ Torr, with the substrate temperature still near room temperature (under 200 °C). The oxygen was then turned off and the heterostructure was annealed in UHV at $\sim 550 °C$ to recrystallize SrTiO$_3$ through a topotactic reaction.[27] Further growth of epitaxial SrTiO$_3$ to the desired film thickness on this recrystallized template was achieved through the repeated codeposition of 5–10 unit cells of amorphous SrTiO$_3$ at room temperature followed by vacuum recrystallization at $\sim 550 °C$. This process is quite time consuming as it involves deposition at low temperature and high (for MBE) oxygen pressure followed by recrystallization at high temperature and UHV. Nonetheless, the resulting epitaxial SrTiO$_3$ films are free from amorphous SiO$_x$ at the SrTiO$_3$/Si interface.

The cross-sectional and plan-view specimens were prepared by standard methods. Cross-sectional specimens were prepared by cutting the film-covered wafer into slices. Two of the slices were glued together face-to-face and embedded in epoxy resin. After the glue was cured, disks with a diameter of 3 mm were obtained by cutting away excess epoxy. These disks were then ground, dimpled, polished, and subsequently argon-ion milled on a stage cooled with liquid nitrogen. For the plan-view specimens only, the substrate sides were thinned by grinding and polishing, followed by dimpling to a thickness of 15 μm and ion milling. TEM and HRTEM investigations were carried out in a JEOL 4000EX electron microscope operated at 400 kV. The compositional homogeneity of the films was investigated by energy-dispersive x-ray (EDX) spectroscopy using a spot size of about 6 nm.

III. RESULTS

The low magnification lattice images of samples A, B, and C, taken with the incident electron beam parallel to the [110] zone axis of the silicon substrates, are shown in Figs. 1(a)–1(c), respectively. The horizontal arrowheads in the images denote the interface between the SrTiO$_3$ thin films and the silicon substrates. The epitaxial nature of the ~ 18- and ~ 10-nm-thick SrTiO$_3$ films from samples A and B, respectively, are evident from Figs. 1(a) and 1(b). No products of interfacial reaction were observed over large areas and the interfaces are free of amorphous phase. No difference in the interface and the film structure could be detected between samples A and B. In contrast, the film/substrate interface in Fig. 1(c) looks rough. An amorphous layer was also observed at the interface of sample C. In addition, crystalline precipitate phases were found along the interface [marked by vertical arrows in Fig. 1(c)]. These precipitates ranged in size from 3 to 10 nm and occurred with an areal density of
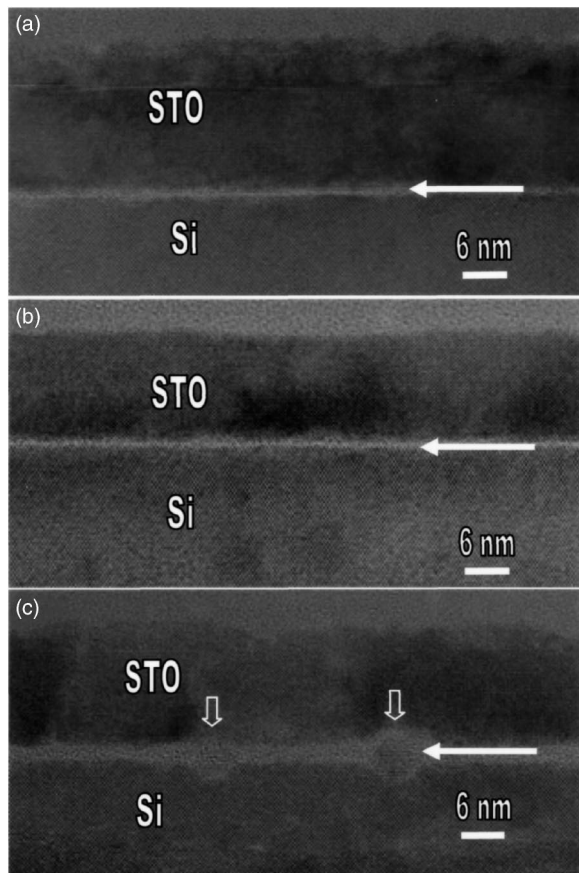
FIG. 1. Cross-sectional low-magnification TEM images of samples A (a), B (b), and C (c). In (a) and (b) sharp and clean interfaces between $SrTiO_3$ films and the silicon substrate are seen, while an amorphous interfacial layer and many nanometer-sized crystalline precipitates are observed in (c).

10^{10}–10^{11} precipitates/cm^2. The EDX analysis showed that the precipitates consisted of titanium and silicon with a Si/Ti ratio close to 2.

Figure 2(a) shows a selected area electron-diffraction (SAED) pattern recorded from a region covering both the $SrTiO_3$ thin film and part of the silicon substrate in sample A. From this pattern, it is clear that the $SrTiO_3$ thin film grows on the silicon substrate with the following crystallographic orientation relationship: $(001)_{SrTiO_3} \| (001)_{Si}$ and $[100]_{SrTiO_3} \| [110]_{Si}$. Figure 2(b) shows an enlarged image of the interface area of Fig. 1(a). It can be seen from Fig. 2(b) that the interface is atomically sharp and the atomic columns in the $SrTiO_3$ thin film are directly linked with those of the silicon substrate. Misfit dislocations are observed on the film side marked by arrowheads. A Burgers circuit around a dislocation leads to a Burgers vector of $a[100]$ in the $SrTiO_3$ for the misfit dislocations, where a is the lattice constant of the $SrTiO_3$.[37] The linear density of misfit dislocations at the $SrTiO_3/Si$ interface, about 3×10^5 misfit dislocations per cm, is found to agree with that calculated from the lattice mismatch between the $SrTiO_3$ thin film and the silicon substrate. These epitaxial $SrTiO_3$ films are fully relaxed.

Figure 3(a) shows an SAED pattern of sample C. The two sets of diffraction spots marked by arrowheads indicate that parts of the $SrTiO_3$ film deviate from perfect epitaxial alignment. Figure 3(b) shows a high magnification image of
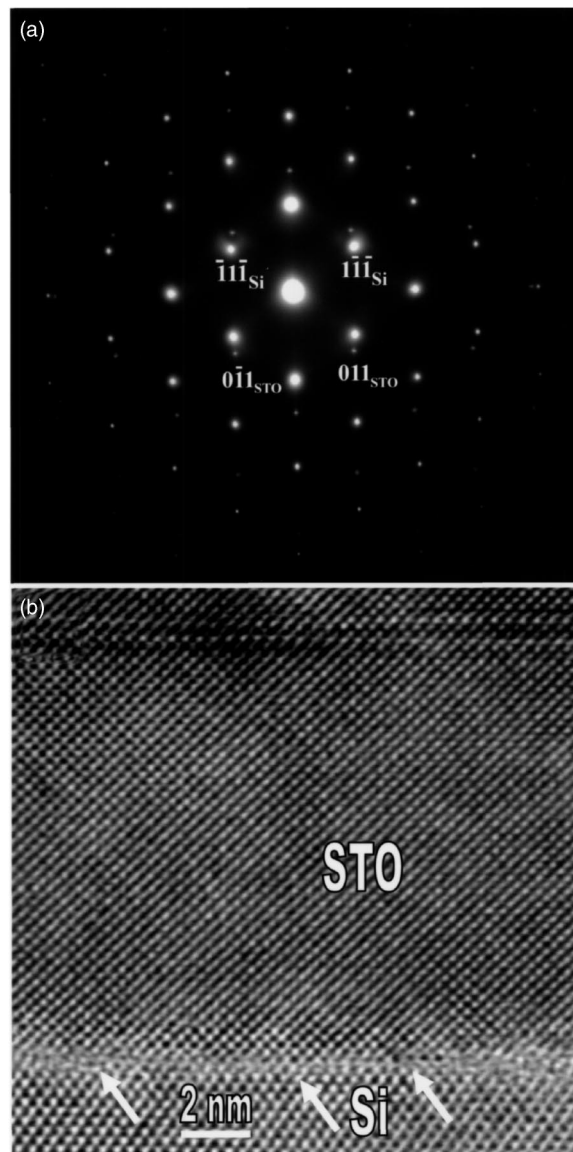

FIG. 2. (a) Selected area electron-diffraction pattern of sample A taken from an interface region indicating a perfect epitaxial relationship between the $SrTiO_3$ film and the silicon substrate. (b) Enlarged lattice image showing a sharp interface between the $SrTiO_3$ thin film and the silicon substrate.

the interface region of sample C. An amorphous layer ~0.8 nm in thickness can clearly be seen. Two precipitates marked by the letter "A" at the $SrTiO_3/Si$ interface show a different structure from $SrTiO_3$ and silicon. The $SrTiO_3$ film shows strong columnar growth features. In Fig. 3(b), three columns are distinguished by two dotted lines in the film. The orientation of the middle column is quite different from its two neighbors.

In order to identify the structure of the precipitates, we investigated them by SAED and HRTEM. According to the EDX analysis, the precipitates are found to have composition $TiSi_2$. $TiSi_2$ has two structural forms: a stable orthorhombic face-centered structure ($C54$) with lattice parameters $a=0.8254$ nm, $b=0.4783$ nm, and $c=0.8540$ nm and a metastable orthorhombic base-centered structure ($C49$) with lattice parameters $a=0.3721$ nm, $b=1.468$ nm, and $c=0.3683$ nm.[38] Figure 4(a) shows a SAED pattern obtained
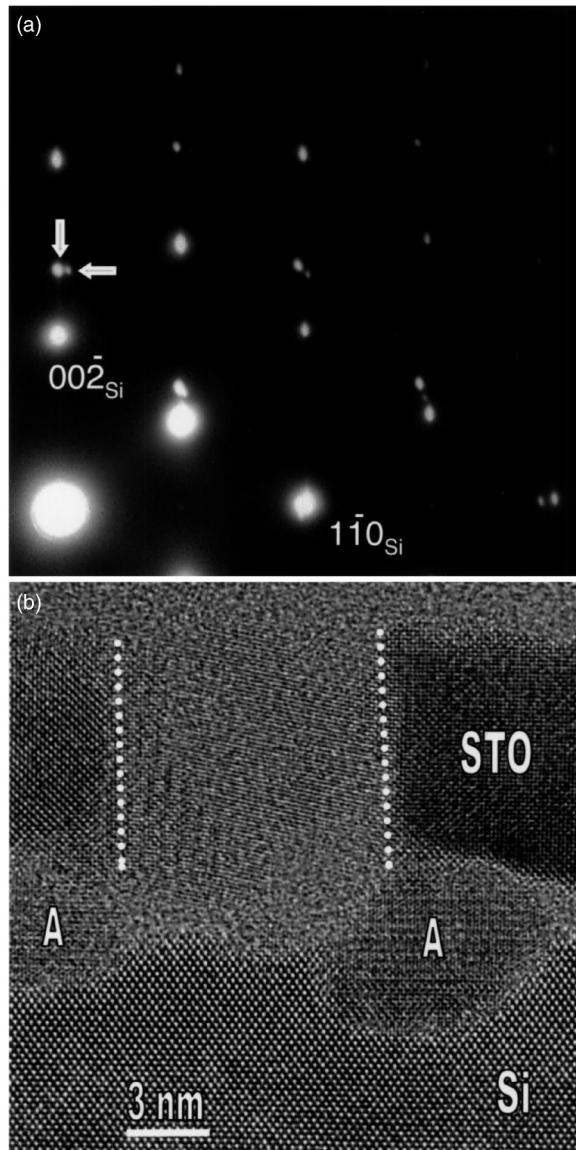
FIG. 3. (a) SAED pattern of sample C showing misorientation of the SrTiO$_3$ film. (b) Cross-sectional TEM lattice image showing grain boundaries between columnar grains of the film. An amorphous layer and two precipitates occur at the interface.

using an aperture encompassing part of the SrTiO$_3$ film, a precipitate, and part of the silicon substrate along its [110] zone axis. In this pattern, the strong spots are the reflections of the silicon substrate. The spots with intermediate intensity are the reflections from the SrTiO$_3$ film. The weak and regularly arranged spots denoted by a rectangular box (indicating tetragonality) and short arrowheads are the reflections from the TiSi$_2$ precipitate. Using the silicon lattice parameter as a calibration standard, the weak diffraction spots can be indexed according to the C49 TiSi$_2$ structure. The existence of the metastable C49 phase rather than the stable C54 phase at room temperature is understandable considering the fact that the C49 TiSi$_2$ is the stable phase (from 200 to 600 °C)[39] at the film growth temperature. Statistical studies on the films showed that these precipitates follow three orientation relationships with the silicon substrate. They are

$$[110]_{Si}\|[001]_{TiSi_2},(001)_{Si}\|(010)_{TiSi_2}, \tag{1}$$

$$[110]_{Si}\|[001]_{TiSi_2},(001)_{Si}\sim\|(100)_{TiSi_2},(about\ 5\,°\ deviation), \tag{2}$$

and

$$[110]_{Si}\|[001]_{TiSi_2},(001)_{Si}\sim\|(310)_{TiSi_2}. \tag{3}$$

Among the three relationships, (1) was most commonly observed due to it having the lowest strain energy. Based on the in-plane orientation determined by maximizing the number of coincidence sites at the interface between TiSi$_2$ and the silicon substrate, the areal mismatch (ΔA) is defined by $\Delta A = A[(\Delta a/a)+(\Delta b/b)+(\Delta\alpha\cot\alpha)]$,[40] where a and b are the edges of the superlattice, α is the angle between the edges of the superlattice a and b, A is equal to $ab\sin\alpha$, and Δa, Δb, and $\Delta\alpha$ are the mismatch of a, b, and α, respectively. The areal mismatch between silicon and the C49 polymorph of TiSi$_2$ based on the above expression is 1.65, 5.69, and 3.12 Å^2, for the orientation relationships (1)–(3), respectively. Figures 4(b)–4(d) show lattice images of the TiSi$_2$ precipitates with the three orientations. The images are taken along the [110] zone axis of the silicon substrate. Lattice defects such as stacking faults are also observed and are denoted by the arrowheads in Figs. 4(c) and 4(d).

IV. DISCUSSION

Our results above show that the microstructure of the SrTiO$_3$ films on silicon and the SrTiO$_3$/Si interfaces depend strongly on the Sr/Ti flux ratio. In addition to forming an amorphous interfacial layer, the excess titanium in the films also results in the formation of TiSi$_2$ precipitates. The TiSi$_2$ precipitates originate from a chemical reaction between the film and the silicon substrate because they are observed only at the interfaces.

For understanding the interfacial reaction, we consider the stability of SrTiO$_3$ and its binary oxide constituents, i.e., SrO and TiO$_2$, in contact with silicon. Although the thermodynamic calculations for SrO in contact with silicon could not be completed due to the absence of thermodynamic data for SrSi$_2$ and Sr$_3$SiO$_5$, it is possible that SrO and silicon are thermodynamically stable in contact with each other at temperatures in the 300–1200 K range over which relevant thermodynamic data exist.[13,14,41] In contrast, all oxides of titanium, including TiO$_2$, are unstable in contact with silicon[13,14] as exemplified by the reaction[13,42,43]

$$TiO_2 + 3Si \rightarrow TiSi_2 + SiO_2\ (\Delta G°_{1000\ K} = -23.014\ kcal/mol). \tag{4}$$
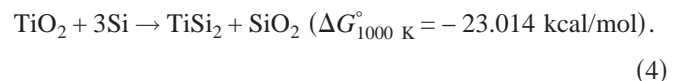
A possible reaction between the SrTiO$_3$ film and the substrate leading to the formation of an amorphous layer along with TiSi$_2$ precipitates is[13,42,43]

$$3Si + SrTiO_3$$
$$\rightarrow SrSiO_3 + TiSi_2\ (\Delta G°_{1000\ K} = -19.133\ kcal/mol). \tag{5}$$
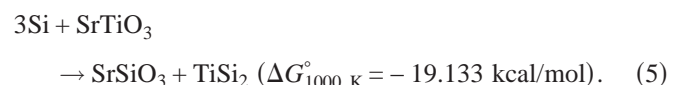
We note that only volume free energies are considered in reactions (4) and (5). While this greatly simplifies calculation
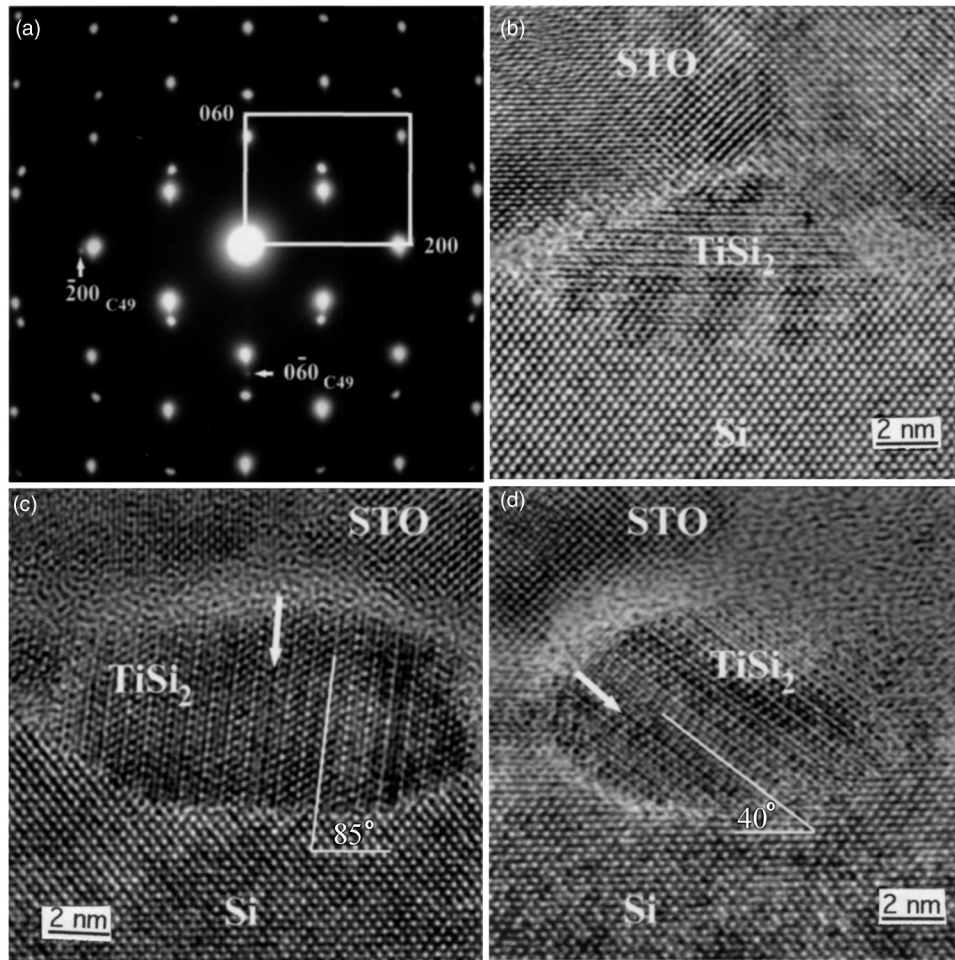
FIG. 4. (a) SAED pattern of C49-TiSi$_2$ together with those of silicon and SrTiO$_3$. (b)–(d) Three differently oriented TiSi$_2$ precipitates at the interface. The arrowheads denote stacking faults in the nanometer-sized precipitates.

of the free energies of reaction, interfacial free energies become important when reactions involving thin reaction layers are involved. The influence of nonbulk contributions, i.e., interfaces and adsorbates, to interfacial reactions can alter the sign of ΔG when its magnitude is close to zero.[44] The free energies of reactions (4) and (5) are sufficiently large, however, they are unlikely to change sign when interfacial energies are considered. The decrease in free energy for reactions (4) and (5) indicates that thermodynamics favors TiSi$_2$ formation at 1000 K, as well as over the entire temperature range (300–1300 K) for which the thermodynamic data for these equations exist. The fact that all three samples were exposed to similar growth temperatures and no SrSiO$_3$ or TiSi$_2$ was detected in samples A and B grown with stoichiometric Sr/Ti flux, excludes the direct reaction of SrTiO$_3$ with silicon [reaction (5)] at growth temperature. The formation of TiSi$_2$ in sample C can therefore be attributed to the reaction between TiO$_2$ and silicon. The excess titanium oxide in the film (as compared to strontium oxide) diffuses to the film/substrate interface, resulting in the formation of amorphous SiO$_2$ and crystalline TiSi$_2$. The amorphous reaction layer at the interface degrades the epitaxy of the subsequent SrTiO$_3$ layers, which leads to the strong columnar structure of the film [see Fig. 3(b)]. The grain boundaries in the columnar film structure act as diffusion pathways for the excess titanium and sustain the interfacial reaction. As film thickness increases, the thickness of the amorphous layer and the size of the TiSi$_2$ precipitates increase.

V. CONCLUSIONS

Epitaxial SrTiO$_3$ thin films grown on (001) Si substrates by MBE were investigated by TEM and HRTEM. The films grown using a stoichiometric Sr:Ti flux ratio flux were epitaxial with no interfacial reaction product. Misfit dislocations were found at the SrTiO$_3$/Si interface having Burgers vector $a[100]$. With excess titanium flux (or insufficient strontium flux), an amorphous interfacial reaction layer a few angstroms thick and crystalline C49 TiSi$_2$ precipitates were observed, probably from the reaction between TiO$_2$ and silicon. Three orientation relationships were observed between the crystalline C49 TiSi$_2$ precipitates at the interface with silicon, of which one is more prevalent because of its better lattice match. The presence of an amorphous interfacial layer affects the epitaxial quality of the SrTiO$_3$ film substantially as evidenced by the columnar film structure.

Our results underscore the importance of accurate composition control for the growth of high-quality SrTiO$_3$ epitaxial films on (001) Si. In the growth of epitaxial-perovskite thin films on oxide substrates, the wide composition space in which single-phase epitaxial films can be grown has been noted.[45] In contrast, our results show the increased importance of accurate composition control when growing on semiconductor substrates, where excess reactants can lead to deleterious reactions with the underlying substrate that negatively impact the ensuing epitaxial microstructure.

[1] S. R. Summerfelt, in *Thin Film Ferroelectric Materials and Devices*, edited by R. Ramesh (Kluwer, Boston, MA, 1997), pp. 1–42.

[2] R. A. McKee, F. J. Walker, and M. F. Chisholm, Phys. Rev. Lett. **81**, 3014 (1998).

[3] K. Eisenbeiser *et al.*, Appl. Phys. Lett. **76**, 1324 (2000).

[4] Z. Yu *et al.*, J. Vac. Sci. Technol. B **18**, 2139 (2000).

[5] R. A. McKee, F. J. Walker, and M. F. Chisholm, Science **293**, 468 (2001).

[6] S. Jeon, F. J. Walker, C. A. Billman, R. A. McKee, and H. Hwang, IEEE Electron Device Lett. **24**, 218 (2003).

[7] F. J. Walker and R. A. McKee, in *High Dielectric Constant Materials: VLSI MOSFET Applications*, edited by H. R. Huff and D. C. Gilmer (Springer, Berlin, 2005), pp. 607–637.

[8] J. Robertson and C. W. Chen, Appl. Phys. Lett. **74**, 1168 (1999).

[9] P. W. Peacock and J. Robertson, Appl. Phys. Lett. **83**, 5497 (2003).

[10] S. A. Chambers, Y. Liang, Z. Yu, R. Droopad, J. Ramdani, and K. Eisenbeiser, Appl. Phys. Lett. **77**, 1662 (2000).

[11] S. A. Chambers, Y. Liang, Z. Yu, R. Droopad, and J. Ramdani, J. Vac. Sci. Technol. A **19**, 934 (2001).

[12] X. Zhang, A. A. Demkov, H. Li, X. Hu, Y. Wei, and J. Kulik, Phys. Rev. B **68**, 125323 (2003).

[13] K. J. Hubbard and D. G. Schlom, J. Mater. Res. **11**, 2757 (1996).

[14] D. G. Schlom and J. H. Haeni, MRS Bull. **27**, 198 (2002).

[15] J. Q. He *et al.*, J. Appl. Phys. **92**, 7200 (2002).

[16] *The National Technology Roadmap for Semiconductors* (Semiconductor Industry Association, San Jose, CA, 1997), p. 72.

[17] G. D. Wilk, R. M. Wallace, and J. M. Anthony, J. Appl. Phys. **89**, 5243 (2001).

[18] J. Lettieri, Ph.D. thesis, Pennsylvania State University, 2002; Available on-line at http://etda.libraries.psu.edu/theses/approved/WorldWideIndex/ETD-202/index.html

[19] H. Li *et al.*, J. Appl. Phys. **93**, 4521 (2003).

[20] H. Mori and H. Ishiwara, Jpn. J. Appl. Phys., Part 2 **30**, L1415 (1991).

[21] B. K. Moon and H. Ishiwara, Jpn. J. Appl. Phys., Part 1 **33**, 1472 (1994).

[22] T. Tambo, T. Nakamura, K. Maeda, H. Ueba, and C. Tatsuyama, Jpn. J. Appl. Phys., Part 1 **37**, 4454 (1998).

[23] T. Tambo, K. Maeda, A. Shimizu, and C. Tatsuyama, J. Appl. Phys. **86**, 3213 (1999).

[24] Y. Liang, S. Gan, and M. Engelhard, Appl. Phys. Lett. **79**, 3591 (2001).

[25] G. Y. Yang *et al.*, J. Mater. Res. **17**, 204 (2002).

[26] X. Hu *et al.*, Appl. Phys. Lett. **82**, 203 (2003).

[27] V. Vaithyanathan, J. Lettieri, J. Haeni, J. Schubert, L. Edge, W. Tian, and D. G. Schlom (unpublished).

[28] D. B. Fenner, A. M. Viano, D. K. Fork, G. A. N. Connell, J. B. Boyce, F. A. Ponce, and J. C. Tramontana, J. Appl. Phys. **69**, 2176 (1991).

[29] C. A. Nordman *et al.*, J. Appl. Phys. **70**, 5697 (1991).

[30] J. A. Alarco, G. Brorsson, Z. G. Ivanov, P.-Å. Nilsson, E. Olsson, and M. Löfgren, Appl. Phys. Lett. **61**, 723 (1992).

[31] G. L. Skofronick, A. H. Carim, S. R. Foltyn, and R. E. Muenchausen, J. Mater. Res. **8**, 2785 (1993).

[32] D. G. Schlom, E. S. Hellman, E. H. Hartford, Jr., C. B. Eom, J. C. Clark, and J. Mannhart, J. Mater. Res. **11**, 1336 (1996).

[33] J. Lettieri, J. H. Haeni, and D. G. Schlom, J. Vac. Sci. Technol. A **20**, 1332 (2002).

[34] C. D. Theis and D. G. Schlom, J. Vac. Sci. Technol. A **14**, 2677 (1996).

[35] Y. Wei *et al.*, J. Vac. Sci. Technol. B **20**, 1402 (2002).

[36] One ML is defined as the concentration of atoms on the (001) surface of silicon, i.e., 6.78×10^{14} at./cm^2.

[37] The Burgers vector is $\frac{a'}{2}[110]$ with respect to the silicon substrate, where a' is the lattice constant of the silicon.

[38] H. Inut, T. Hashimoto, K. Tanaka, I. Tanaka, T. Mizoguchi, H. Adachi, and M. Yamaguchi, Acta Mater. **49**, 83 (2001).

[39] F. J. Himpsel, J. E. Ortega, G. J. Mankey, and R. F. Willis, Adv. Phys. **47**, 511 (1998).

[40] A. S. Yapsir, C. H. Choi, and T. M. Lu, J. Appl. Phys. **67**, 796 (1990).

[41] D. G. Schlom, C. A. Billman, J. H. Haeni, J. Lettieri, P. H. Tan, R. R. M. Held, S. Völk, and K. J. Hubbard (unpublished).

[42] I. Barin and O. Knacke, *Thermochemical Properties of Inorganic Substances* (Springer, Berlin, 1973).

[43] I. Barin, O. Knacke, and O. Kubaschewski, *Thermochemical Properties of Inorganic Substances, Supplement* (Springer, Berlin, 1977).

[44] J. H. Weaver, in *Electronic Materials: A New Era of Materials Science*, Springer Series in Solid-State Science Vol. 95, edited by J. R. Chelikowsky and A. Franciosi (Springer, Berlin, 1991), Chap. 8.

[45] H. Ota, S. Migita, S.-B. Xiong, H. Fujino, Y. Kasai, and S. Sakai, Jpn. J. Appl. Phys., Part 2 **38**, L1535 (1999).